Liquefaction and Reliquefaction Characteristics of Cement Mixing Pile Strengthening Aeolian Sand Subgrade

Yuan Zhou (421163324@qq.com)
Southwest University of Science and Technology https://orcid.org/0000-0002-7565-9366
Honggang Wu
Guizhou University
Zhigang Ma
Southwest University of Science and Technology
Hao Sun
Southwest University of Science and Technology

Research Article

Keywords: Cement mixing pile, Aeolian sand, Shaking table, Liquefaction, Reliquefaction

Posted Date: March 8th, 2022

DOI: https://doi.org/10.21203/rs.3.rs-1403356/v1

Abstract

When the line project passes through a large area of aeolian sand, cement mixing piles are often used to reinforce the subgrade, which can effectively improve the bearing capacity of the subgrade, but its anti-liquefaction effect is worthy of in-depth evaluation. Intermittent earthquakes cause more than one liquefaction of aeolian sand subgrade, so it is worth further research on the re-liquefaction characteristics of cement mixing piles in treatment of aeolian sand subgrade. In this paper, a real-time comparative test (pile reinforced area and unreinforced area) is carried out through a shaking table, and the liquefaction and re-liquefaction characteristics of the reinforced subgrade are mainly explored. The experimental model will produce the following results under 0.4g EL Centro wave excitation:(1) The pore pressure will have multiple peaks, causing the surface of the model to float or sink. The phenomenon will be weakened by experiencing multiple earthquakes of the same level or using pile reinforcement;(2) The deeper the burial depth, the longer the time for the pore pressure to reach the maximum peak value. After multiple vibrations, the corresponding time of the shallow layer in the unreinforced area and the deep layer in the reinforced area doubles;(3) The cement mixing pile can improve the liquefaction and re-liquefaction resistance of aeolian sand foundation, and the effect is best in the shallow foundation, with an increase of more than 30%, and the deeper the burial depth, the lower the effect;(4) After the subgrade has experienced a strong earthquake, its resistance to liquefaction will be improved, but the acceleration response during the next earthquake will increase significantly.

1 Introduction

Liquefiable sand is widely distributed around the world, and it is inevitable that civil engineering will be built on the sand. When an earthquake occurs, liquefaction will cause surface subsidence, and the effective stress state of the soil will approach 0, causing massive damage to surface structures and underground foundations. Most studies on sand liquefaction focus on the initial liquefaction. However, earthquakes occur repeatedly in history, and relevant examples show that aftershocks and two strong earthquakes separated by many years can cause liquefaction again (Wakamatsu 2012; Huang and Yu 2013; El-Sekelly 2017), that is reliquefaction phenomenon. After an earthquake, the density of sand increases with the discharge of pore water and surface subsidence. Olson et al. (2001;2005) demonstrated that the reliquefaction resistance will increase accordingly. Based on data compiled by Mesri et al.(1990) from ground improvement projects, liquefaction resistance may increase after the relative density increases on the order of 20–30%. In addition, even if the sediments have the same initial density, the sand that has undergone pre-shock has greater stability, which contributes to the improvement of liquefaction resistance (Su et al 2013; Teparaksa and Koseki 2018). However, some scholars have proposed that the seismic history reduces the reliquefaction resistance of sand despite a significant increase in sand density(Wahyudi et al .2016; Morimoto et al .2019; Iwai et al .2020). Yamada(2010) and Ha(2011) believed that the anisotropy and density of sandy soil jointly affect the reliquefaction phenomenon. When the anisotropy dominates, the liquefaction will be intensified. Otherwise, the reliquefaction resistance will increase. Wang (2019) also obtained the same result by

numerical DEM test of 2D polydisperse circular particle material with liquefaction history. Finn et al. (1970) concluded that the liquefaction resistance increases if a small shear strain is applied before the cyclic loading test, whereas the liquefaction resistance decreases when the relevant soil is pre-applied with a large shear strain. El-Sekelly (2014,2018) also found that the previous earthquake history has a signficant effect on changing the liquefaction resistance of sandy sediments. His centrifuge experiment results showed that most historical earthquakes can improve the liquefaction resistance of sandy soils, but some larger earthquakes reduce it completely or partially. With the advancement of monitoring technology, scholars have a deeper understanding of the reliquefaction problem at the microscopic level.Ye et al.(2018) used a stereo microscope and an industrial camera, combined with digital image processing technology, to obtain meso-parameters indicating that the long-axis direction of the sand particles developed from the horizontal direction in the initial state to the vertical direction after liquefaction, and the reliquefaction resistance decreased. Xie et al.(2021) used a microscopic image acquisition system to observe the changes in the mesostructure of sand bodies under repeated seismic liquefaction events, and concluded that repeated vibrations improved the compactness of sediments, thus increasing the chance of sand grains contacting each other, opening pores and the generation of elongated pores are less.So,it has a more positive effect on the reliquefaction resistance of sand bodies.

The author of this paper filled the sand model with pile reinforcement and unreinforced area indoors, and built embankment on the model surface. The shaking table simulates the occurrence of earthquake history, and uses sensors to record the dynamic response of the model under the excitation of three strong earthquakes (including surface subsidence, pore water pressure and acceleration). Finally, the liquefaction and re-liquefaction characteristics of aeolian sand subgrade are analyzed based on macroscopic phenomena and data collection results, and the positive role of cement mixing piles in it is expounded.

2 Shaking Table Testing Program And Conditions

2.1 Shaking table

This test was carried out in the geotechnical test hall of Southwest Jiaotong University. The shaking table and its supporting control system were produced by Suzhou Sushi Testing Group Co., Ltd., model SV-1212. The size of the shaking table was 1.2m×1.2m, the maximum load is 0.5t, the working frequency range is 2 ~ 1250Hz, the peak value of horizontal acceleration is 4.37g, and the maximum displacement is ± 51mm. It can output various regular waves, random waves and artificial simulated seismic waves. The test uses a tempered glass model box, the internal size of which is 1m × 0.4m × 0.8m, and the glass side walls are conducive to observing the macroscopic phenomenon of the test. In addition, in order to reduce the influence of reflected waves from rigid walls, the short side walls of the model box (perpendicular to the vibration direction) are affixed with 15cm thick foam boards.

2.2 Testing material

The test sand in this study is aeolian sand widely distributed along the Sichuan-Tibet Railway in China. The sand has fine particles, no viscosity, poor water retention, and strong water sensitivity and dynamic vulnerability. The particle size of aeolian sand is mainly distributed in 0.25 mm ~ 0.074 mm, the maximum dry density is 1.5 g/cm^3, and the maximum saturation density is 1.9 g/cm^3. Figure 1 shows the grain size distribution curve of aeolian sand, which includes the sand liquefaction limit proposed by Tsuchida (1970), and the aeolian sand is within this range.

The purpose of shaking table test is to generate the real response of the prototype through the proportional model. The similarity ratio between the prototype and the model is worthy of careful consideration. Limited by the load of the shaking table and the size of the model box, the geometric similarity ratio is 1 : 20 in this experiment. According to the previous research basis (Ling et al. 2004), this paper selects the geometric size L, mass density ρ and elastic modulus E as the model control variables. This shows that the dynamic duration ratio of model loading is 1 : 1, because the duration of earthquake without similar ratio compression is better for liquefaction test, otherwise it may lead to no liquefaction of foundation(Xu et al.2019). Its physical quantities are derived from the Bockingham π theorem, as shown in Table 1

2.3 Test model making

Taking the on-site construction of a certain aeolian sand road section as a prototype, the model cement mixing pile has a pile diameter of 2.5cm, a pile length of 50cm, a pile spacing of 6cm after conversion by similarity ratio. In order to visually compare the liquefaction and re-liquefaction characteristics of the aeolian sand subgrade strengthened by cement mixing piles, the model box was divided into two halves along the vibration direction to form a piled area and a pileless area. ore water pressure and acceleration sensors are arranged at different depths of the subgrade (shallow, middle, and deep layers). The model design and sensor arrangement are shown in Fig. 2.

The specific preparation process of the model is as follows: (1)The prefabricated cement mixing pile is carried out through the plastic pipe mold, and the thin iron rod is used for uniform mixing while pouring, and the mold is removed after standing for 7 days.（2）The foundation is filled in layers and compacted by hammering. During the whole process, the pile is inserted and the sensor is arranged. The position of the pile is positioned by the thin foam board with positioning holes; （3）After the foundation reaches the target depth, slowly inject water into the model to saturate the roadbed. The change of the water level inside the model can be observed through the tempered glass on the side until the water level reaches the surface of the roadbed, and the model foundation can be considered to be in a saturated state for 24 hours. （4）Construction of embankments and installation of laser displacement meters. It is worth noting that: in order to prevent the laser of the displacement meter from being affected by the surface water, the displacement measuring points are set on both sides of the embankment. The test details are shown in Fig. 3.

2.4 Test plan

In this test, the seismic wave was loaded in the X direction, and the waveform was selected from the seismic waveform widely used by experts and scholars in the field of earthquake research at home and abroad - EL Centro wave. This wave is a seismic wave with a maximum acceleration of more than 300 gal that was first captured in the United States in 1940 (Ikuo T 1996), and the waveform is shown in Fig. 4 It should be pointed out that, since this experiment focuses on the dynamic response between sand and soil-pile systems, combined with the previous research foundation, the use of the original waveform input has little effect on the research purpose of this experiment, so the seismic wave input has not been processed for similarity ratio(Cesca and Grigoli 2014). The foundation reliquefaction is studied under the condition of damage accumulation, so by designing the continuous case to induce multiple liquefaction of the foundation, as in the subsequent analysis of the results, case 1 (GK1) is sufficient to induce the first liquefaction event in the model. In the subsequent design of working conditions, historical earthquakes were simulated by using multiple vibration events (there is enough time between earthquakes to allow water pressure to dissipate and consolidate, and the interval time is not less than 40 minutes), including strong earthquakes and aftershocks. The specific loading sequence of seismic waves is shown in Fig. 5. Since this paper focuses on the comparative study of the liquefaction and re-liquefaction characteristics of cement-mixed piles strengthening aeolian sand subgrade, the influence of three strong earthquakes of the same magnitude (GK1, GK2, GK13) on the model is mainly analyzed.

3 Analysis Of Test Results

3.1 Macroscopic phenomenon

Under the excitation of strong earthquakes, the main macroscopic phenomena of the experimental model are incline subsidence of embankment, ground subsidence and surface water effluent. Figure 6 is a simplified diagram of the macroscopic phenomena of the model under different working conditions. As the picture shows: the unreinforced aeolian sand subgrade was greatly affected by the earthquake. The first strong earthquake (GK1) caused a significant subsidence of the surface of the area, about 3 mm, and a 1 mm water level was formed. After the second strong earthquake (GK2), the subsidence expanded to 5 mm, The water level developed to 2mm, and the third strong earthquake (GK13) only deepened the water level to 3mm. For the area reinforced by cement mixing piles, the ground surface settles by 2mm only at GK1, and a water level of 1mm is formed after GK2, while GK13 has no obvious effect on this area. In addition, it can be found that the unreinforced side embankment sinks into the ground, the reinforced side embankment settles synchronously with the ground surface, and the effect of piles to improve the integrity of the subgrade is remarkable. Combined with the settlement curves on both sides of the embankment in Fig. 7, the settlement of W2 increases significantly compared to W1, which is consistent with the macroscopic phenomenon, that is, the embankment is continuously inclined and subsided to the unreinforced area under strong earthquakes.

In Fig. 7, GK1 caused W1 to subside by 2mm, which is consistent with the surface subsidence in this area. Subsequent earthquakes did not intensify the subsidence of W1, but the curve fluctuated slightly.On the other hand, W2 subsides 4mm under the action of GK1, and it is worth noting that the curve rises to

the peak and then drops instantaneously, indicating that the unreinforced aeolian sand subgrade is more prone to obvious "instantaneous expansion and contraction" phenomenon, resulting in the embankment rising and falling. Subsidence, W2 also has this feature in GK2, and the subsidence amount reaches 7mm, and the small fluctuation of the curve reflects the expansion and contraction characteristics of the entire model under the action of earthquake. Under the action of a series of aftershocks (GK3□GK12), W2 floated up, and the subsequent strong earthquake (GK13) caused W2 to sink to 7mm, but there was no substantial expansion and contraction of the subgrade. Perhaps the alternation of large and small earthquakes is the internal cause of the expansion and contraction of the model subgrade. To sum up, the aeolian sand subgrade reinforced with cement mixing piles has strong ability to resist multiple strong earthquake damage, can effectively restrain the surface subsidence, and prevent the earthquake subsidence of surface structures.

3.2 Pore pressure ratio

Figure 8 shows the time history of the pore-pressure ratio (excess static pore water pressure/initial overlying earth pressure) recorded at different depths of the model during the three strong earthquakes. A pore-pressure ratio greater than 1 indicates that liquefaction occurred in this area. In order to illustrate the initial change process of the pore pressure ratio in more detail, the graph is plotted with logarithmic coordinates on the horizontal axis, and two important time periods are marked in the figure, namely the arrival time of liquefaction(The time period during which the pore pressure ratio increases from 0 to 1) and liquefaction duration (The time period from the first time the pore pressure ratio reaches 1 to the last time it reaches 1). As shown in Fig. 8: (1)For the whole model, the growth trend of the pore-pressure ratio is closely related to the buried depth of the measuring point.

The fastest growth is at 30 cm, followed by 50 cm, and the growth is not obvious at 10 cm. The corresponding rule is that the middle of the model is the most likely to liquefy, followed by the bottom, and the shallow layers are less affected by the earthquake. The reason for the above results is that the shallow sand is close to the surface, the pore water penetrates to the surface of the foundation faster, and the pore water pressure measured in the deep foundation is large, but the weight of the sand column between the piles is also large, and the corresponding overlying earth pressure value is high., so the pore pressure ratio of the two increases relatively slowly. (2)Focusing on the initial stage of the pore pressure ratio time history curve, there is a phenomenon of "instantaneous negative pore pressure" at each measuring point. The main reason is that due to the "instantaneous expansion" effect of the model when the initial acceleration peak is reached, the pore water pressure meter measures the suction force instead of the pressure instantaneously, that is, the instantaneous record of the pore pressure is a negative value. It can be seen from the two important time period changes of the pore-pressure ratio time-history curve at the burial depth of 30cm: the change rule under the three strong earthquakes is that the first strong earthquake causes the sand layer to reach liquefaction time is short, about 0.41s, and liquefaction duration up to 11.69s, but the two subsequent strong earthquakes both prolonged the time to liquefaction and shortened the duration of liquefaction to varying degrees. In addition, compared with the unreinforced area, the cement mixing piles in the first two strong earthquakes can effectively prolong the

liquefaction time in the middle of the aeolian sand subgrade and reduce the liquefaction duration, but in the third strong earthquake, this advantage is not obvious. (4) Obviously, the pore pressure at the depths of 30 cm and 10 cm does not increase and dissipate regularly under the excitation of 0.4 gEL wave, but has multiple instantaneous peaks. The macroscopic representation is described as sand boiling, which is also the reason for the expansion and contraction of the model subgrade.

Figure 8 focuses on the liquefaction time in the middle of the model. The shallow and deep layers did not liquefy during the whole test, but the time point at which the peak appeared can also be used as an evaluation index for the liquefaction time. Therefore, based on Fig. 8, a histogram of the time required for the pore pressure to go from 0 to the peak value (hereinafter referred to as the peak time) at different measuring points of the model under different working conditions (Fig. 9). In GK1, the peak time of aeolian sand subgrade increases with the deepening of burial depth, and the reinforced subgrade shows the same law and delays this time. Under the GK2 event, what changed was that the peak time was shortened at a depth of 30 cm in the reinforced area, and the subsequent GK13 event continued to shorten this time. On the other hand, the peak time of the unreinforced area did not change. For GK13, the obvious difference is that the peak time of the shallow layer in the unreinforced area and the deep layer in the reinforced area is doubled, indicating that a series of aftershocks after the strong earthquake can effectively prolong the liquefaction time in these two areas.

In order to directly reflect the liquefaction and reliquefaction characteristics of the model at different burial depths, the pore-pressure ratio peak map under three strong earthquakes was drawn (Fig. 10). It can be clearly seen from the figure that the peak value of the pore-pressure ratio of all measuring points of the second strong earthquake is smaller than that of the first strong earthquake. The results of the third strong earthquake were different.During the third strong earthquake, the peaks of L1 and L4 (50cm buried depth), L2 and L5 (30cm buried depth) continued to decline,but the observation points L3 and L6 (buried depth 10cm) have risen. It may be that the surface water level formed and the pore water accumulated in the shallow sandy soil inhibited the dissipation of pore water pressure, resulting in an increase in the peak pore pressure ratio.

Both the macroscopic phenomenon and the time-history curve of the pore-pressure ratio prove that the cement-mixed pile can improve the liquefaction resistance of the aeolian sand foundation. n order to quantitatively reflect this capability, based on the peak pore pressure ratio at the same buried depth in the piled area and the unpiled area, the improvement ratio δ of the liquefaction resistance of the cement mixing pile is defined.The formula is as follows.

$$\delta = \left| \frac{v^{'} - v_0}{v_0} \right| \times 100\%$$

In the formula: $v_0$is the peak value of the pore pressure ratio in the pile-free area, and $v^{'}$ is the peak value of the pore pressure ratio between the piles at the same burial depth. Figure 11 shows the relationship of

δ under three strong earthquakes. As shown in the figure, on the whole, the cement mixing pile has the best anti-liquefaction effect on the shallow layer of the model foundation, and the value of δ is above 30%, and even reached 57.6% in GK2. The effect of the development of the middle layer of the foundation is greatly weakened, and the effect continues to weaken slightly when it continues to the deep layer. In particular, for GK2, the pile body has the weakest anti-liquefaction effect in the middle of the model, where δ is 0.7%, which is equivalent to no pile reinforcement. It is possible that the large subsidence of the surface in the unreinforced area caused by the first strong earthquake increased the compactness of the central part, enhanced the occlusal force between the aeolian sand particles, and formed a more stable structure, which can be equal to the liquefaction resistance of the central part of the reinforced area. Comparing GK1 to GK13, the delta value of 30cm buried depth dropped from 13.3–6.5%, the 50cm buried δ value dropped from 10.2–5.9%, and the shallow buried depth of 12cm increased from 30.2–47.4%, indicating that after many earthquakes (including strong earthquakes and aftershocks), the liquefaction resistance of the cement-mixed piles in the middle and deep foundations of the model will be reduced, and the shallow layers will be improved.

3.3 Acceleration response

Figure 12 and Fig. 13 respectively show the acceleration time-history curve and the acceleration peak response of the measurement points at different buried depths of the model under three strong earthquakes. In Fig. 12, In particular, the acceleration response waveform buried in the shallow layer of the unreinforced area is different from the input wave. This is because the shallow sand is under low overburden pressure and is in a loose state, so it is easy to be disturbed by the earthquake, and the accelerometer data is disturbed during the acquisition. However, it can be found that the waveform of GK2 has a certain stability, because the compactness of this area has been improved after the first strong earthquake, and the data acquisition state tends to be stable. The horizontal dotted line in Fig. 13 is the peak line of table acceleration collected when 0.4gEL Centro wave is input. Figure 13 shows that the different buried depth measurement points in the model have an amplification effect on the acceleration, and the relationship is proportional to the height of the measurement point from the table. For the same buried depth, the peak value of the acceleration response in the reinforced area is much larger than that in the unreinforced area. It can be seen that the interaction between the pile structure and the aeolian sand subgrade has a strong response to the dynamic force. It can be clearly seen that, compared with the previous strong earthquake, the acceleration response peak value of each measuring point of each subsequent strong earthquake has increased.

The above studies show that although the soil layer may have improved liquefaction resistance after undergoing the sand liquefaction process. However, this improvement in liquefaction resistance is accompanied by a significant increase in the dynamic response of the soil layer during the next earthquake, which may lead to a significant increase in the degree of damage to buildings built within or above it.

4 Conclusion

The anti-liquefaction (including liquefaction and re-liquefaction) effects of cement-mixed piles reinforced aeolian sand subgrade were evaluated by carrying out the shaking table test under EL Centro wave excitation. The dynamic response law of the subgrade under multiple excitations of the same magnitude earthquake is revealed, and the main conclusions are as follows:

(1) During the earthquake action, due to the multiple instantaneous peaks of pore pressure, the aeolian sand subgrade will expand and contract, causing the surface or embankment to float and sink. This phenomenon will be weakened after repeated earthquakes or pile reinforcement.

(2) From the pore-pressure ratio time-history curve, it can be seen that the liquefaction law of the aeolian sand foundation with pile reinforcement and without piles is the same. The middle of the foundation is the most likely to liquefy, the deep layer is subject to the largest effective stress of the overlying layer, followed by the liquefaction characteristics of the earthquake, and the shallow layer is less affected due to the short drainage path to the surface.

(3) The time for the pore pressure of the entire model to reach its peak value is proportional to the depth of the aeolian sand subgrade. The deeper the burial depth, the longer the time. After multiple earthquakes, the law remains unchanged, but the corresponding time of the shallow layer in the unreinforced area and the deep layer in the reinforced area doubles.

(4) The cement mixing pile can improve the liquefaction resistance of the aeolian sand foundation. The effect is best in the shallow layer of the foundation, with an increase of more than 30%. The characteristics are greatly weakened in the middle, and slightly weakened in the deep layer. The performance is inversely proportional to the depth of the subgrade. The effect is best in the shallow layer of the foundation, with an increase of more than 30%. Its characteristics are greatly weakened in the middle of the development, and it continues to weaken slightly in the deep layer. The performance is inversely proportional to the depth of the subgrade.

(5) After the soil layer has undergone the process of sand liquefaction, its resistance to liquefaction will be improved. However, this improvement in liquefaction resistance is accompanied by a significant increase in the dynamic response of the soil layer during the next earthquake, which may lead to a significant increase in the degree of damage to buildings built within or above it.

Declarations

Acknowledgements This article belongs to the Science and Technology Development Program of China Railway Corporation Limited（2018- Key plan -45）, and this work was supported by the Independent Innovation Fund of China Railway Northwest Research Institute (XBYKY2018901001).

Affiliations

Yuan Zhou[1,2] Honggang Wu[2] Zhigang Ma[1,2] Hao Sun[1,2]

Honggang Wu

271462550@qq.com

Zhigang Ma

1415025990@qq.com

Hao Sun

973680437@qq.com

1 School of Civil Engineering and Architecture, Southwest University of Science and Technology, Mianyang 621010, China

2 Northwest Railway Academy Co.,Ltd. of CREC,Lanzhou,Gansu730000,China

References

1. Cesca S (2014) **Grigoli F(2014) Full waveform seismological advances for microseismic monitoring. Advances in Geophysics 56(12): 169–228. https://doi.org/10.1016/bs.agph.12.002**
2. El-Sekelly (2014) **W() The effect of seismic preshaking history on the liquefaction resistance of granular soil deposits [Ph.D. Dissertation]. Troy, NY: Rensselaer Polytechnic Institute**
3. El-Sekelly W, Dobry R, Abdoun T (1943) **Steidl JH(2017) Two case histories demonstrating the effect of past earthquakes on liquefaction resistance of silty sand. J Geotech Geoenviron Eng 143(6):04017009. https://doi.org/10.1061/(ASCE)GT.-5606.0001654**
4. El-Sekelly W, **Mercado V, Abdoun T H,**. et al (2018) **() Contraction and pore pressure behavior of a silty sand deposit subjected to an extended shaking history. Soil Dynamics and Earthquake Engineering, 114:215–224. https://doi.org/10.1016/j.soildyn.2018.07.023**
5. Finn W **P.L. Bransby, and D.J. Pickering(1970) Effect of strain history on liquefaction of sand. Journal of Soil Mechanics & Foundations Div,96(SM6)**
6. Ha IS, Olson SM, Seo MW, Kim MM (2011) **() Evaluation of reliquefaction resistance using shaking table tests. Soil Dyn Earthq Eng 31(4):682–691. https://doi.org/10.1016/j.soildyn.2010.12.008**
7. Huang Y, Yu M (2013) **() Review of soil liquefaction characteristics during major earthquakes of the twenty-first century. Nat Hazards 65(3):2375–2384. https://doi.org/10.1007/s11069-012-0433-9**
8. Ikuo T (1996) **() Seismic wave propagation in elastic soil with continuous variation of shear modulus in the vertical direction. Soils and Foundations 36(1): 61–72. https://doi.org/10.3208/sandf.36.61**
9. Ling Xianchang (2004) **Wang Chen, Wang Cheng(2004) Similar design method of shaking table test model for dynamic interaction of pile-soil-bridge structure in liquefaction site. Chinese Journal of Rock Mechanics and Engineering, 2004(03): 450–456. https://doi.org/10.3321/j.issn:1000-6915.03.017**

10. Iwai H, Ni X, Ye B, Nishimura N, Zhang F (2020) () A new evaluation index for reliquefaction resistance of Toyoura sand. Soil Dynam Earthq Eng;136: 106206. https://doi.org/10.1016/j.soildyn.2020.106206
11. Mesri G, Feng TW Benak JM(1990) Postdensification penetration resistance of clean sands. J Geotech Eng 116(GT7):1095–115. https://doi.org/10.1016/0148-9062(91)93426-7
12. Morimoto T, Aoyagi Y, Koseki J (2019) () Effects of induced anisotropy on multiple liquefaction properties of sand with initial static shear. Soils Found 59(6):2024–2035. https://doi.org/10.1016/j.sandf.2019.03.015
13. Olson SM, Obermeier SF Stark TD(2001) Interpretation of penetration resistance for back-analysis at sites of previous liquefaction.Seismol Res Lett72(1):46–59
14. Olson SM, Green RA (2004) Obermeier SF(2005) Geotechnical analysis of paleoseismic shaking using liquefaction effects: a major updating. Eng Geol 76(3–4): 235–261. https://doi.org/10.1016/j.enggeo.07.008
15. Su D, Ming HY (2013) Li XS(2013) Effect of shaking strength on the seismic response of liquefiable level ground. Eng Geol 166(8):262–271. https://doi.org/10.1016/j.enggeo.09.013
16. Tsuchida H (1970) () Prediction and countermeans against the liquefaction in sand deposits. Abstract of the Seminar in the Port and Harbor Research Institute,Yokohama, Japan, 3.1–3.33
17. Teparaksa J, Koseki J (2018) () Effect of past history on liquefaction resistance of level ground in shaking table test. G´eotech Lett 8(4):256–61. https://doi.org/10.1680/jgele.18.00085
18. Wakamatsu K (2012) () Recurrence of liquefaction at the same site induced by the 2011 Great East Japan Earthquake compared with previous earthquakes. Paper presented at the 15th world conference on earthquake engineering Lisbon, Portugal
19. Wahyudi S, Koseki J, Sato T, Chiaro G (2016) () Multiple-liquefaction behavior of sand in cyclic simple stacked-ring shear tests. Int J GeoMech 16(5):C4015001. https://doi.org/10.1061/(ASCE)GM.1943-5622.0000596
20. Wang R, Fu P, Zhang JM, et al (2019) () Fabric characteristics and processes influencing the liquefaction and re-liquefaction of sand. Soil Dynamics and Earthquake Engineering 125(Oct.):105720.1-105720.11. https://doi.org/10.1016/j.soildyn.2019.105720
21. Xu Chengshun, Dou Pengfei, Gao Yancheng, (2019) Shaking table test of the influence of the duration compression ratio of ground motion on the seismic response of liquefiable foundations. Rock and Soil Mechanics 40(1): 147–155. https://doi.org/10.16285/j.rsm et al (2017) 2342
22. Xiaoli Xie, Bin Ye, Teng Zhao,. et al (2021) ()Changes in sand mesostructure under repeated seismic liquefaction events during centrifuge tests. Soil Dynamics & Earthquake Engineering 150:106940. https://doi.org/10.1016/j.soildyn.2021.106940
23. Yamada S, Takamori T Sato K(2010) Effects on reliquefaction resistance produced by changes in anisotropy during liquefaction. Soils and Foundations 50(1): 9–25. https://doi.org/10.3208/sandf.50.9

24. Ye B, **H Hu**, **Bao X**,. et al (2018) **() Reliquefaction behavior of sand and its mesoscopic mechanism**. **Soil Dynamics and Earthquake Engineering 114**:12–21. **https://doi.org/10.1016/j.soildyn.2018.06.024**

Tables

Table 1 Similar Ratio Design for Shaking Table Test

Physical quantity	Physical symbol	Similarity	Similarity ratio
Geometry	L	S_L	1/20
Mass density	ρ	S_ρ	1
Elastic modulus	E	S_E	1/20
Acceleration	g	$S_g = 1$	1
Linear displacement	s	$S_s=S_L$	1
Self-weight of upper embankment	P	$S_P=S_L^3$	$1/20^3$
Dynamic duration	T	$S_T=1$	1
Pore water pressure	μ	$S_\mu=S_L$	1/20

Figures

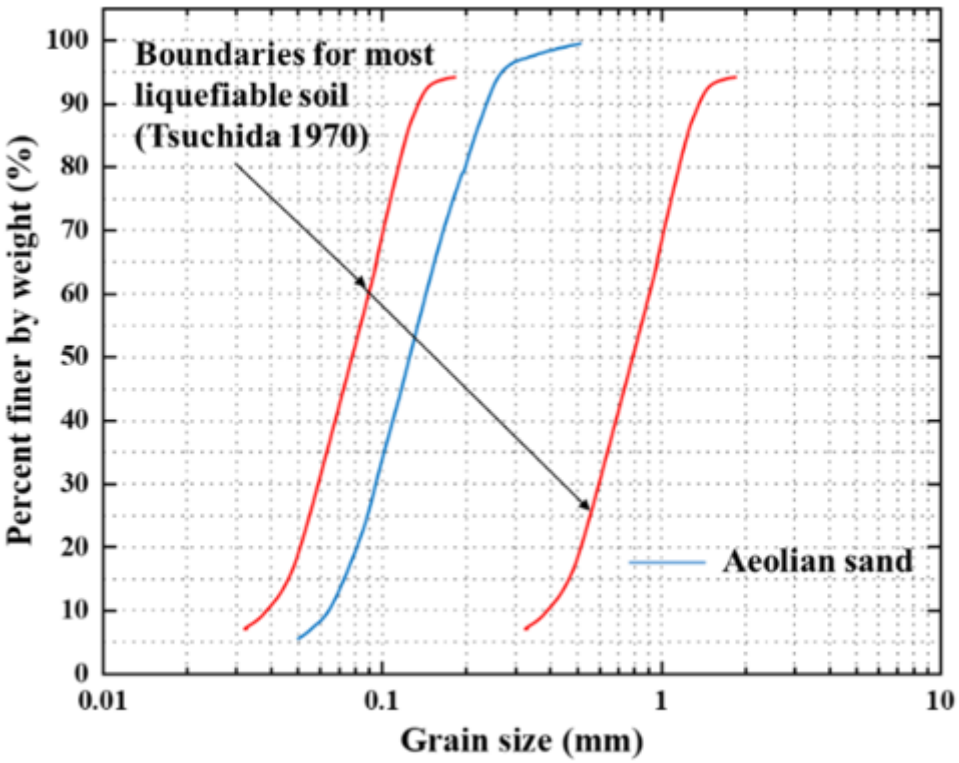

Figure 1

Grain size distributions of aeolian sand

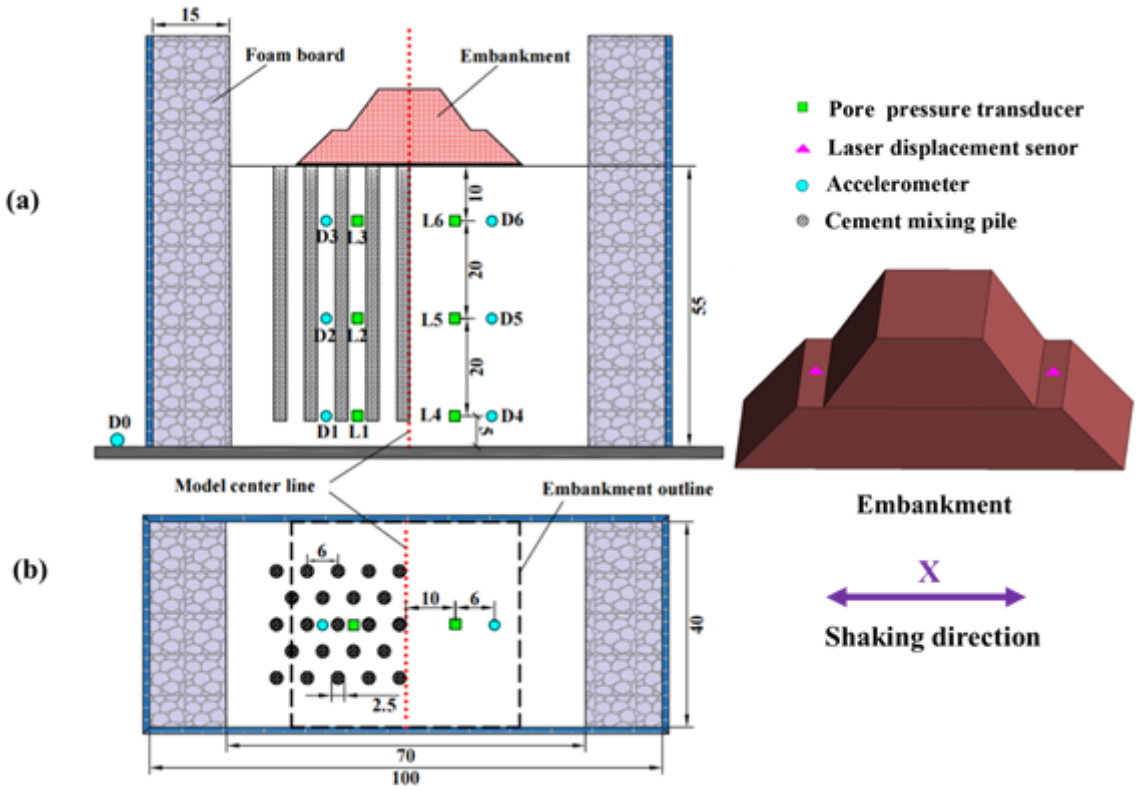

Figure 2

Model design and sensor arrangement

(a) model front view (b) Model top view

Figure 3

Test details

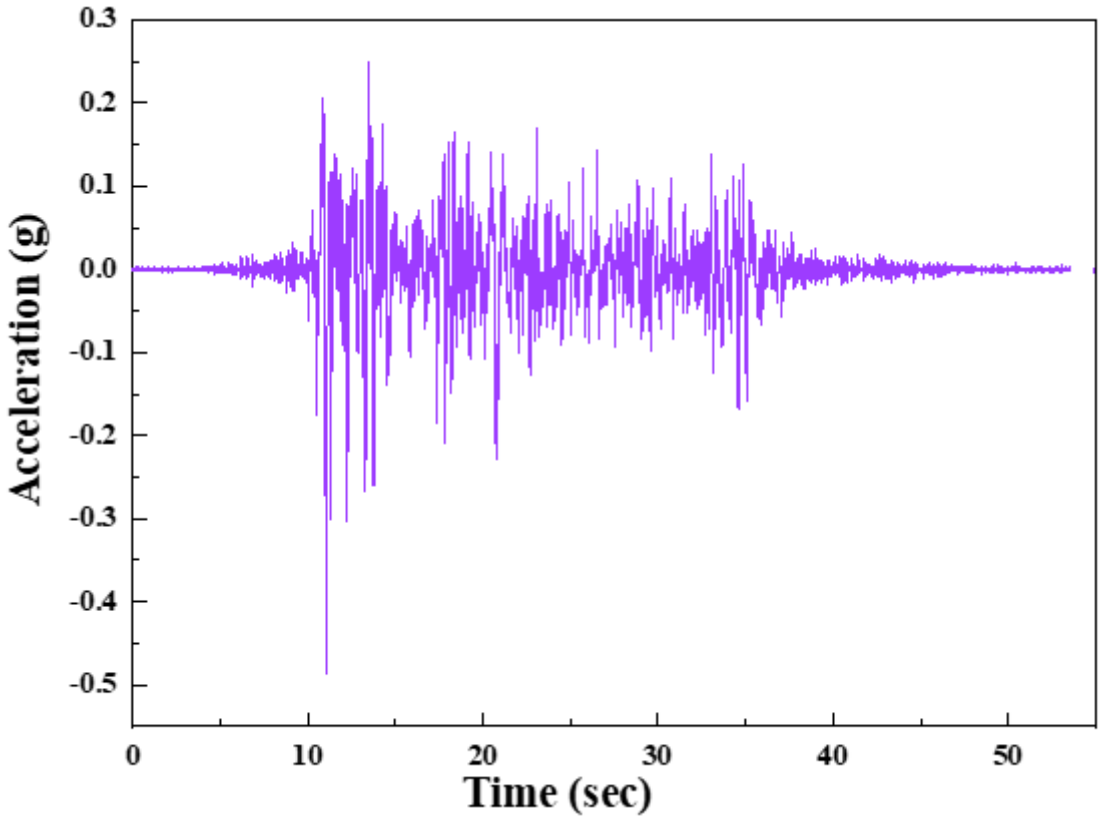

Figure 4

EL Centro wave acceleration time-history curve

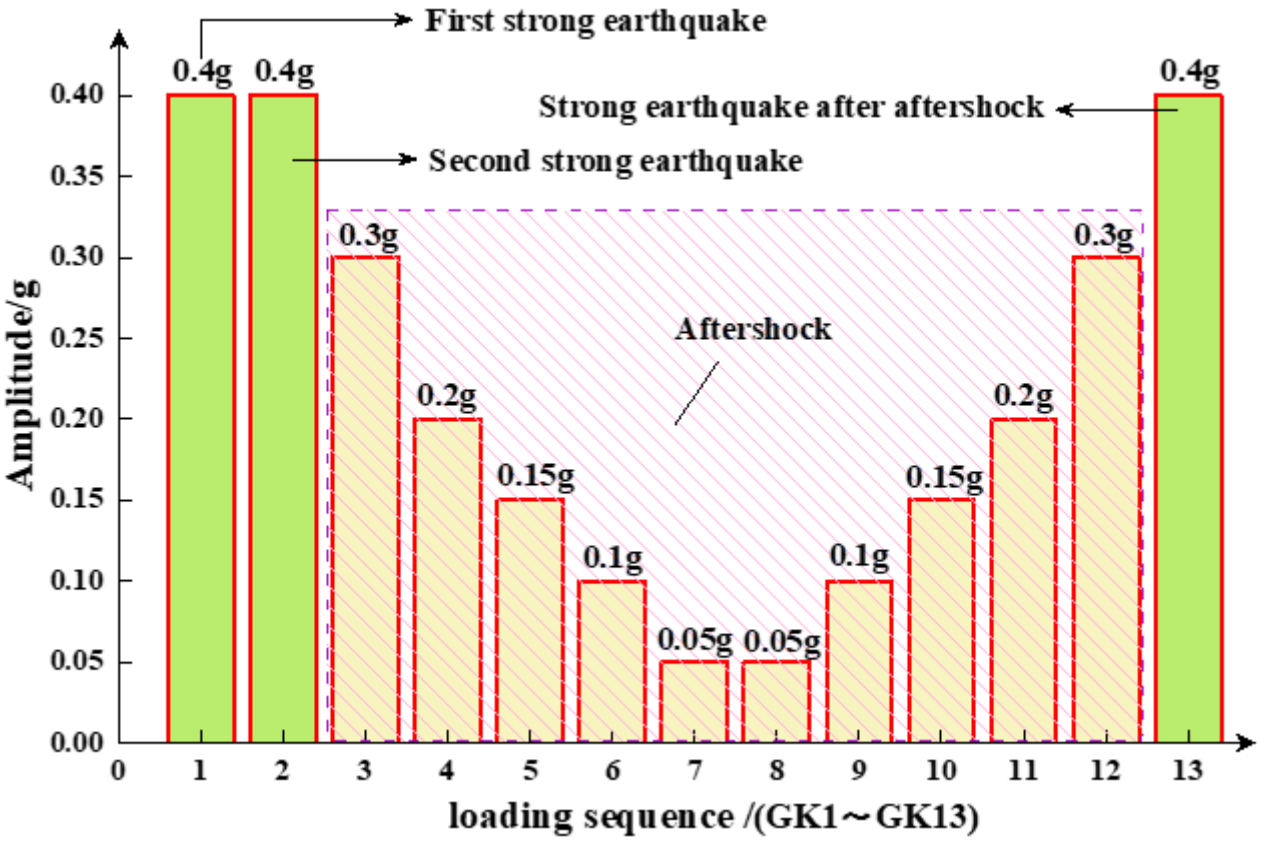

Figure 5

Load order

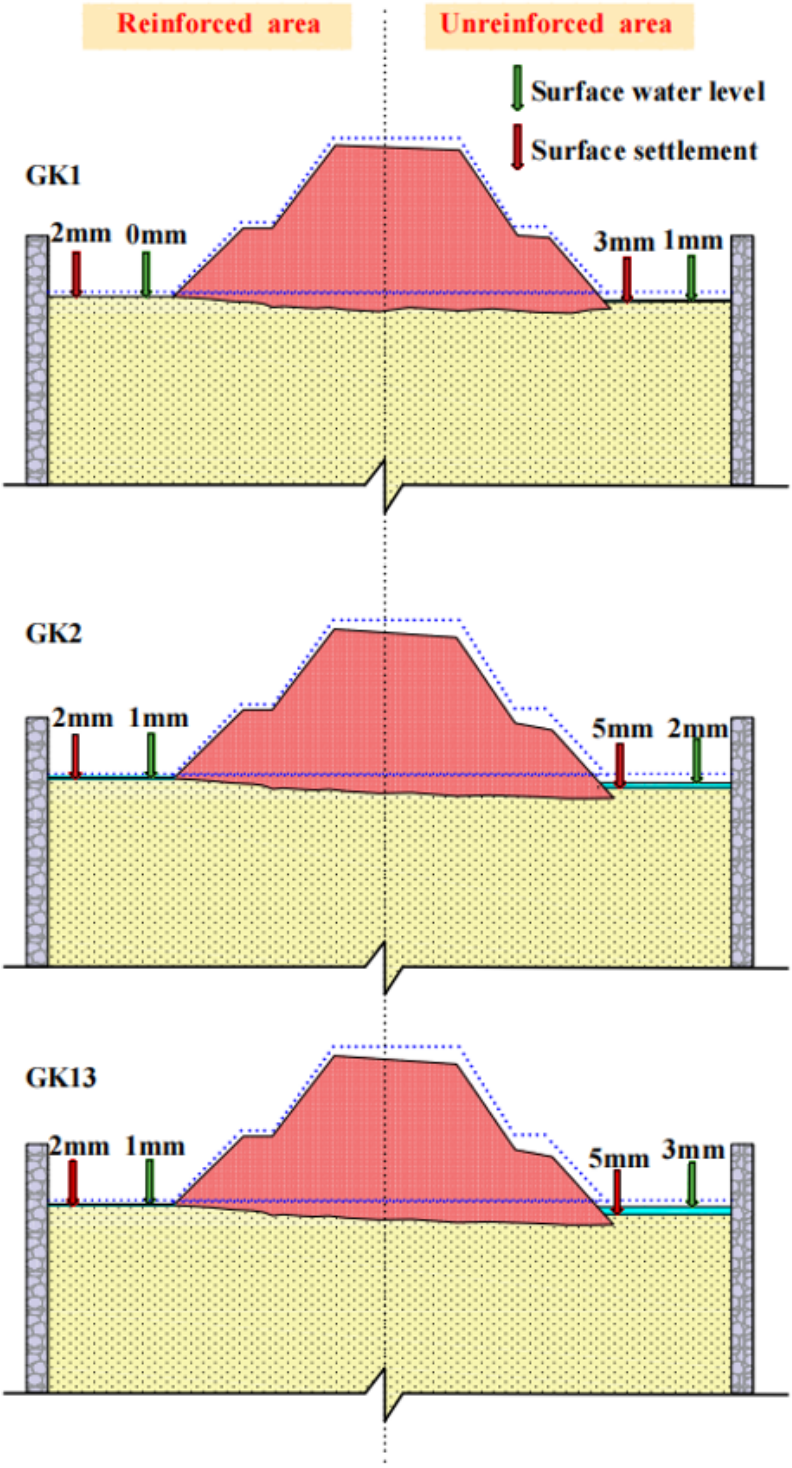

Figure 6

Sketch map of macroscopic phenomena

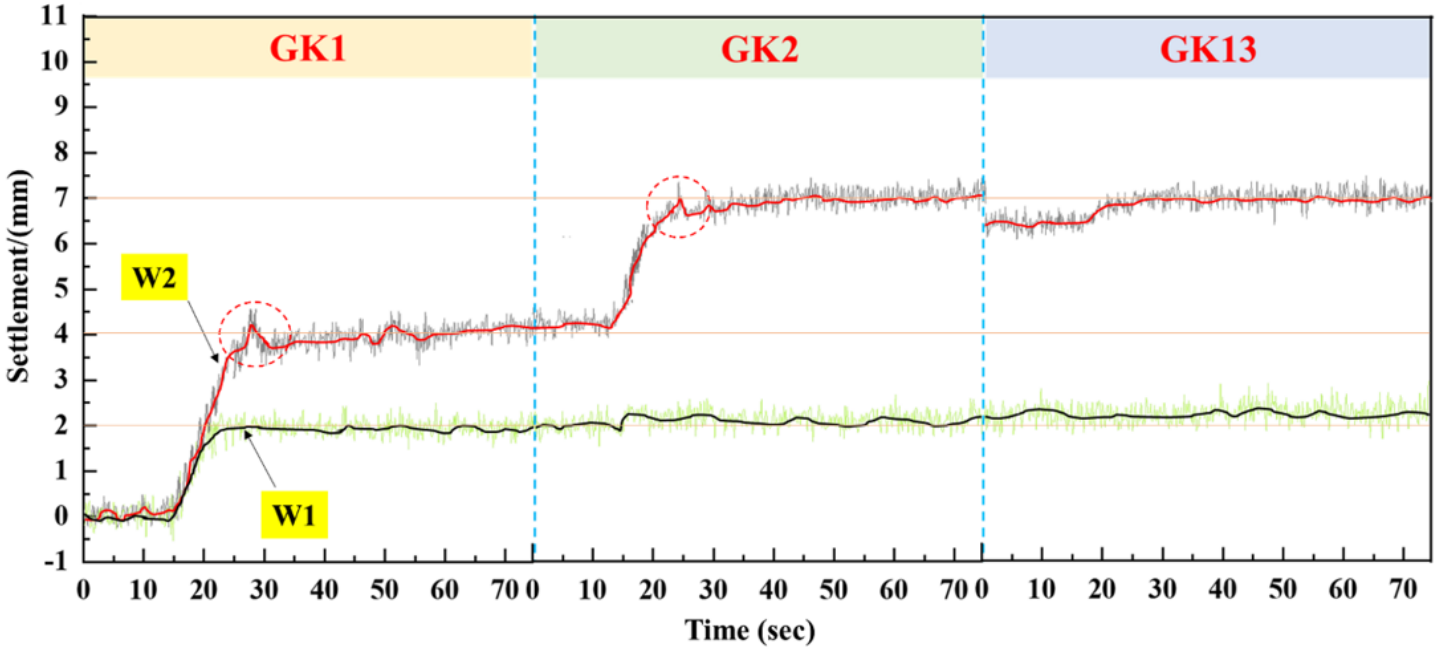

Figure 7

Embankment settlement curve

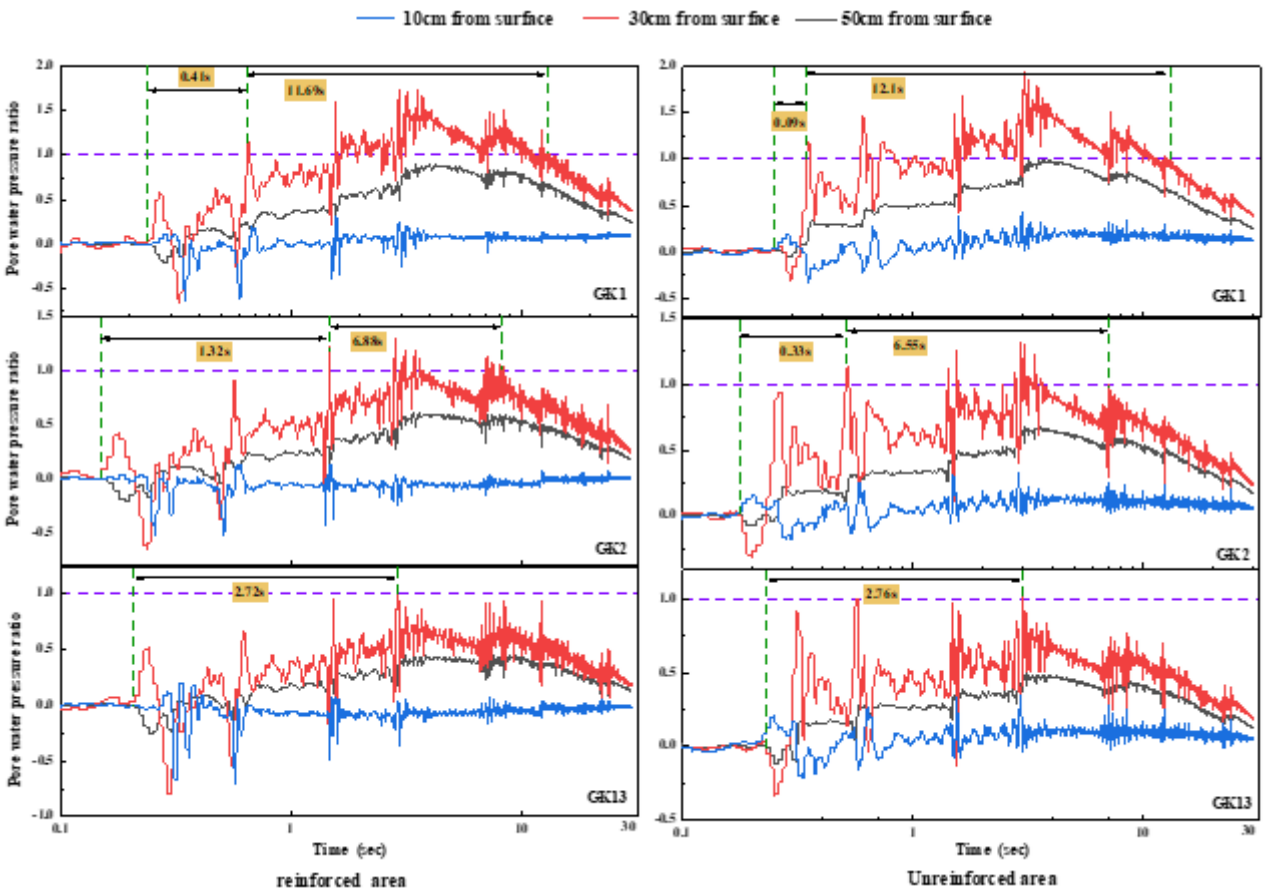

Figure 8

Time history curve of pore pressure ratio

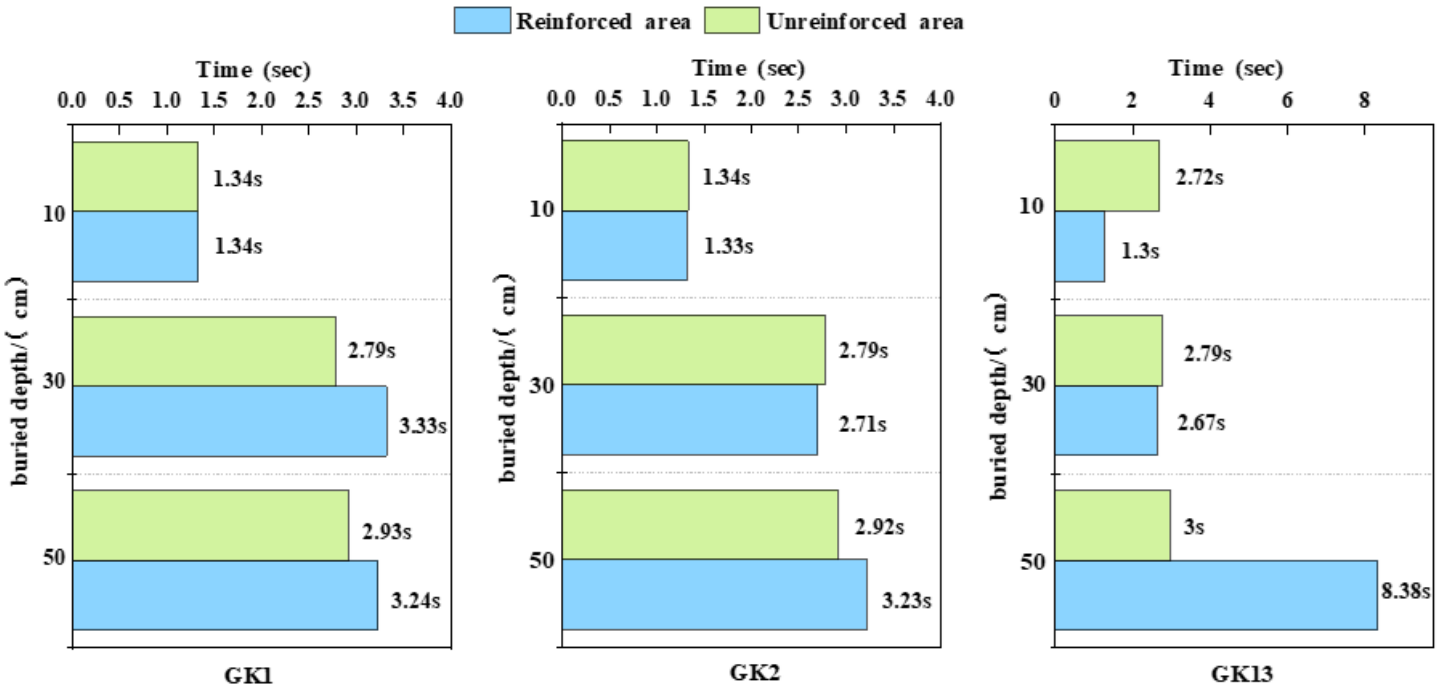

Figure 9

Time required for pore pressure at different measuring points to reach peak value

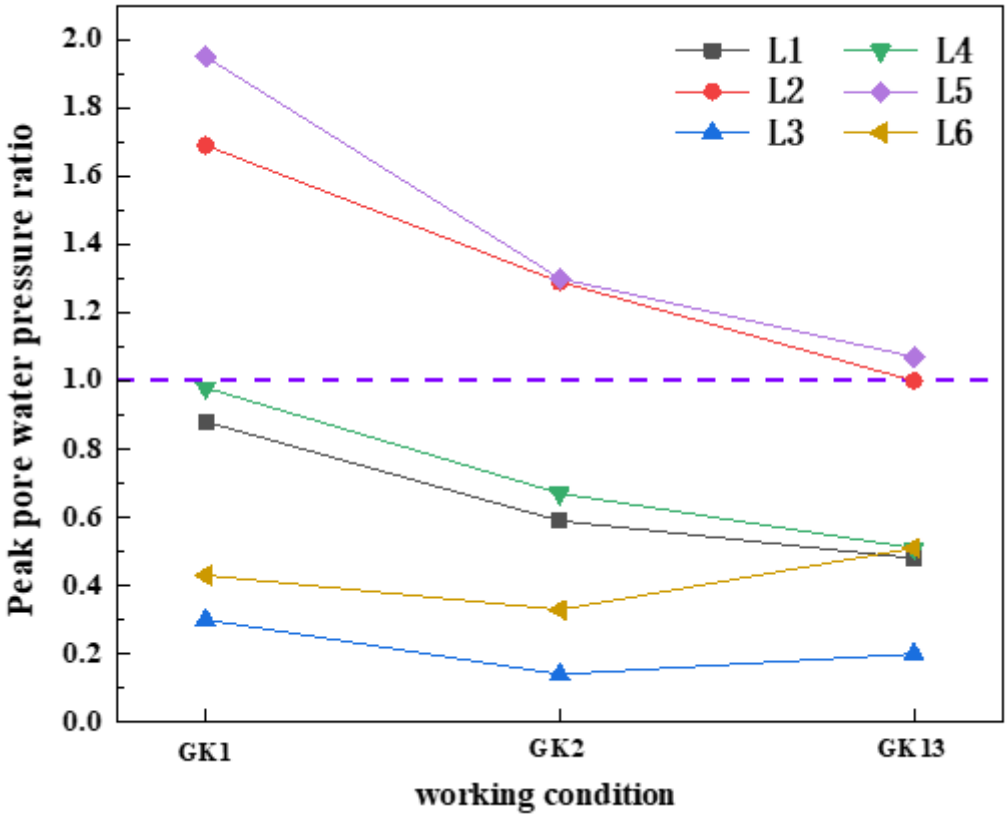

Figure 10

Peak curve of pore pressure ratio

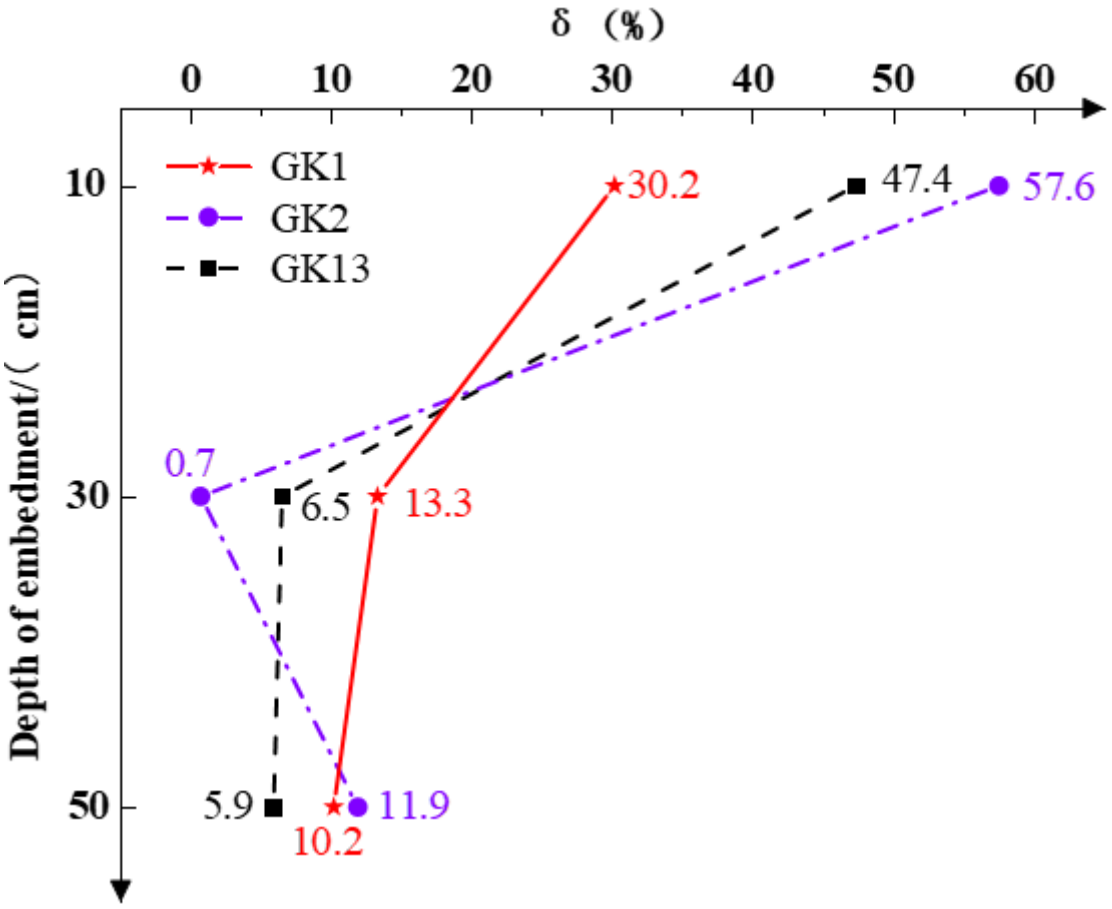

Figure 11

Curve of anti-liquefaction lifting ratio of cement mixing pile

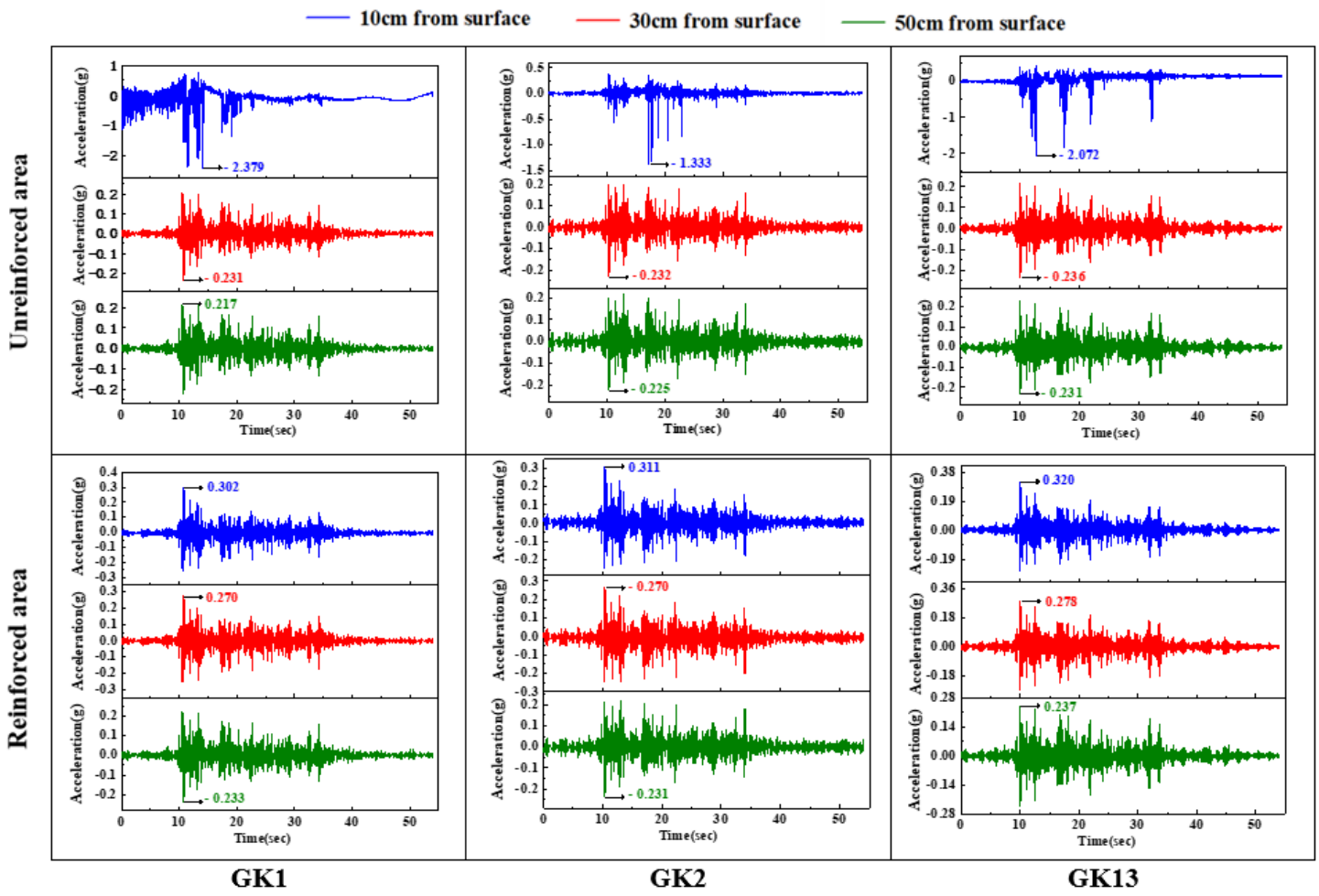

Figure 12

Acceleration time-history curve

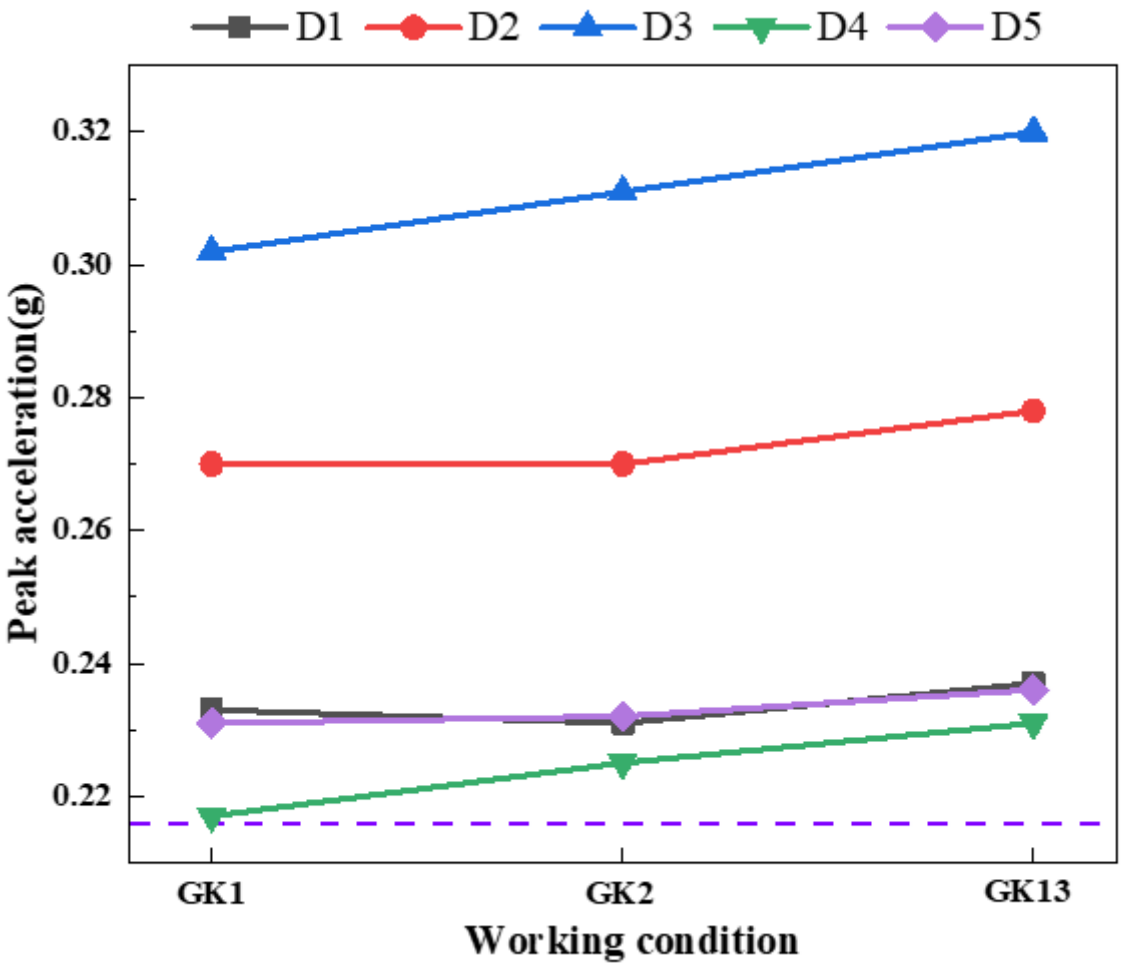

Figure 13

Acceleration peak curve